Cite as: M. A. Bandres *et al.*, *Science* 10.1126/science.aar4005 (2018).

Topological insulator laser: Experiments

Miguel A. Bandres,[1]* Steffen Wittek,[2]* Gal Harari,[1]* Midya Parto,[2] Jinhan Ren,[2] Mordechai Segev,[1]† Demetrios N. Christodoulides,[2]† Mercedeh Khajavikhan[2]†

[1]Physics Department and Solid State Institute, Technion, Haifa 32000, Israel. [2]CREOL, College of Optics and Photonics, University of Central Florida, Orlando, FL 32816, USA.

*These authors contributed equally to this work.

†Corresponding author. Email: msegev@techunix.technion.ac.il (M.S.); demetri@creol.ucf.edu (D.N.C.); mercedeh@creol.ucf.edu (M.K.)

Physical systems exhibiting topological invariants are naturally endowed with robustness against perturbations, as manifested in topological insulators—materials exhibiting robust electron transport, immune from scattering by defects and disorder. Recent years have witnessed intense efforts toward exploiting these phenomena in photonics. Here, we demonstrate a nonmagnetic topological insulator laser system exhibiting topologically protected transport in the cavity. The topological properties give rise to single mode lasing, robustness against defects, and significantly higher slope efficiencies compared to the topologically trivial counterparts. We further exploit the properties of active topological platforms by assembling the system from S-chiral microresonators, enforcing predetermined unidirectional lasing without magnetic fields. This work paves the way toward active topological devices with unique properties and functionalities.

Topological insulators are a phase of matter featuring an insulating bulk while supporting conducting edge states (*1*–*3*). Remarkably, the transport of edge-states in topological insulators is granted topological protection, a property stemming from the underlying topological invariants (*2*). For example, in two-dimensional systems the ensued one-way conduction along the edge of a topological insulator is by nature scatter-free—a direct outcome of the nontrivial topology of the bulk electronic wavefunctions (*3*). Although topological protection was initially encountered in the integer quantum Hall effect (*4*), the field of topological physics developed rapidly after it was recognized that topologically-protected transport can also be observed even in the absence of a magnetic field (*5*, *6*). This in turn, spurred a flurry of experimental activities in a number of electronic material systems (*7*). The promise of robust transport inspired studies in many and diverse fields beyond solid-state physics, such as optics, ultracold atomic gases, mechanics and acoustics (*8*–*23*). Along these lines, unidirectional topological states were observed in microwave settings (*24*) in the presence of a magnetic field (the electromagnetic analog of the quantum Hall effect), while more recently topologically-protected transport phenomena have been successfully demonstrated in optical passive all-dielectric environments by introducing artificial gauge fields (*13*, *25*).

In photonics, topological concepts could lead to new families of optical structures and devices by exploiting robust, scatter-free light propagation. Lasers in particular, could directly benefit from such attributes [see (*26*)]. In general, laser cavities are prone to disorder, which inevitably arises from fabrication imperfections, operational degradation and malfunction. Specifically, the presence of disorder in a laser gives rise to spatial light localization within the cavity, ultimately resulting in a degraded overlap of the lasing mode with the gain profile. This implies lower output coupling, multimode lasing, and reduced slope efficiency. These issues become acute in arrays of coupled laser resonators (used to yield higher power), where a large number of elements is involved. Naturally, it would be of interest to exploit topological features in designing laser systems that are immune to disorder. In this spirit, several groups have recently studied edge-mode lasing in topological 1D Su-Schrieffer-Heeger resonator arrays (*27*–*29*). However, being one-dimensional they lase in a zero-dimensional defect state, which inherently cannot provide protected transport. On the other hand, two-dimensional (2D) laser systems can directly benefit from topological protection. Indeed, it was shown theoretically that it is possible to harness the underlying features of topological insulators in 2D laser arrays—when lasing in an extended topological state (*26*, *30*, *31*). As indicated there, such systems can operate in a single mode fashion with high slope efficiencies in spite of appreciable disorder. In a following development, unidirectional edge-mode lasing was demonstrated in a topological photonic crystal configuration involving a YIG substrate under the action of a magnetic field (*32*). In that system, lasing occurred within a narrow spectral bandgap induced by magneto-optic effects. Clearly, it would be of interest to pursue magnet-free approaches that are by nature more compatible with fabrication procedures and photonic integration involving low-loss components. In addition, such all-

dielectric systems can prove advantageous in substantially expanding the topological bandgap, and in doing that bring the topological protection of photon transport to the level that lasing is immune to defects and disorder.

Here, we report the first observation of topologically-protected edge-mode lasing in nonmagnetic, two-dimensional topological cavity arrays. We show that this topological insulator laser can operate in single mode, even considerably above threshold, with a slope efficiency that is significantly higher than that achieved in their corresponding trivial realizations. Moreover, we observe experimentally that the topological protection leads to more efficient lasing than for the trivial counterpart, even in the presence of defects. Finally, to show the potential of this active system, we assemble a topological system based on S-chiral resonator, which can provide new avenues to control the topological features.

Design of the topological insulator laser

We fabricate a 10 × 10 coupled ring-resonator array on an active platform involving vertically stacked 30 nm thick InGaAsP quantum wells [see (*33*), Fig. 1A]. We couple the array to a waveguide that acts as an output coupler which allows us to interrogate the system using out-coupling gratings (Fig. 1B, corresponding to the yellow framed regions in Fig. 1A). The active lattice investigated here uses a topological architecture suggested in (*26*), which is based on adding gain and loss to the topological passive silicon platform demonstrated in (*10*). This 2D setting comprises a square lattice of ring resonators which are coupled to each other via link rings (Fig. 1, A and C). The link rings are designed so as to be antiresonant to the main ring resonators. In this all-dielectric design, the intermediary links are judiciously spatially-shifted along the y-axis, with respect to the ring resonators, to introduce an asymmetric set of hopping phases. The phase shift is sequentially increased along the y-axis in integer multiples of $\pm 2\pi\alpha$, designed here to be $\alpha = 0.25$. In this way, a round trip along any plaquette (consisting of 4 rings and 4 links) results in a total accumulated phase of $\pm 2\pi\alpha$, where the sign depends on the direction of the path along this unit cell. This provides the lattice with a synthetic magnetic field and establishes two topologically non-trivial bandgaps. The cross-section of each ring (500 nm width and 210 nm height) is designed to ensure single transverse mode conditions at the wavelength of operation 1550 nm (*33*). The nominal separation between the ring-resonators and off-resonant links is 150 nm, thus leading to two frequency bandgaps, each having a width of 80 GHz (0.64 nm). The spectral size of the two bandgaps was obtained by experimentally measuring the frequency splitting (0.8 nm) in a binary system of primary resonators, linked via an intermediate racetrack ring [see (*33*), Part 9]. In order to promote protected edge-mode lasing, we optically pump only the outer perimeter of this array at 1064 nm with 10 ns pulses (Fig. 1D). This is achieved using a set of appropriate amplitude masks (supplementary materials, Part 1). The intensity structure of the lasing modes is captured using an InGaAs infrared camera, and their spectral content is then analyzed using a spectrometer with an array detector (*33*). In what follows we compare the features of the topological insulator lasers ($\alpha = 0.25$) with those of their trivial counterparts ($\alpha = 0$) under various conditions.

Studying the features of the topological insulator laser

The edge mode can be made to lase by pumping the boundary of the topological array (*26*). In this case, a clear signature of topological lasing would be highly efficient single-mode emission even at gain values high above the threshold. To observe these features in experiments, we pump the perimeter of the topological and trivial arrays, and measure the lasing output power (integrated over the two out-coupling gratings) and its spectral content. The light-light curves measured for the topological and the trivial arrays (Fig. 2A) clearly show that the topological system lases with a higher efficiency than its trivial counterpart. From their measured spectra (Fig. 2, B and D), we observe that the topological arrays remain single-moded over a wide range of pumping densities (Fig. 2C), whereas the trivial arrays (tested over multiple samples) always emit in multiple wavelengths with considerably broader linewidths (Fig. 2D). Importantly, if we only compare the power emitted in the dominant (longitudinal) mode of the topological array to the mode with the highest power in the trivial array, the topological laser outperforms the trivial one by more than an order of magnitude. This difference in performance is attributed to the physical properties of the topological edge-modes. The trivial array suffers from several drawbacks. First, the trivial lasing modes extend into the lossy bulk, thus experiencing suppressed emission. Second, the trivial lasing modes try to avoid the output coupler so as to optimize their gain. And finally, due to intrinsic disorder in fabrication, the lasing mode localizes in several different parts of the trivial lattice, each lasing at a different frequency, thereby giving rise to a multimode behavior. Conversely, apart from a weak exponential penetration into the bulk, in topological arrays the edge-states are strongly confined to the edge. Moreover, since they forced to flow around the perimeter, they are always in contact with the output coupler. Finally, because of its inherent topological properties, the lasing edge mode does not suffer from localization, and therefore it uniformly extends around the perimeter (in single mode), using all the available gain in the system by suppressing any other parasitic mode.

In order to demonstrate that these active lattices exhibit topological features, we compare their lasing response against

that of their trivial counterparts ($\alpha = 0$) when their periphery is pumped. The emission intensity profiles obtained from these two systems are shown in Fig. 3, B and C. To check whether the lasing modes are extended or localized around the perimeter of the lattice, we measure the spectrum of the light emitted from different sites around the arrays (Fig. 3, A and E). For the trivial array, we observe that the spectrum varies around the lattice, with emission occurring over a wide wavelength range spanning from 1543 nm to 1570 nm, as shown in Fig. 3A. This is an indication that the trivial array lases in localized domains, each one at a different frequency. In sharp contrast, in the topological array, all sites emit coherently at the same wavelength (Fig. 3E). Such lasing, in a single extended topological edge mode, is a direct manifestation of topologically-protected transport. These results are consistent with those presented in Fig. 2. Topological transport in these structures is further investigated by selectively pumping the lattice. First, we pump only one edge of the 2D array, as depicted in Fig. 3D, inset. Under these conditions, the lasing mode in the trivial system is confined to the pumped region (Fig. 3D). In this arrangement, the emission is heavily suppressed both in the bulk as well as along the perimeter and consequently no light is extracted from any of the output grating couplers. In contrast, for the topological array, even when only one side is pumped, the edge mode flows along the periphery—finally reaching the output coupler, as shown in Fig. 3H. In this case, only one output coupler grating emits strongly. This indicates that the lasing mode that reaches the output coupler has a definite chirality in each ring. Given that the emission is in a single mode, one can conclude that lasing takes place in only one topological mode. To show that in the topological case it is the edge mode that lases, while in the trivial case the bulk states lase, we expand the pumping region at the right edge (Fig. 3C, inset). In the trivial case, even though pumping over a larger area is now provided, still no laser light reaches the output ports (Fig. 3C). That means that there are no traveling edge modes that could reach the output ports. On the other hand, for the topological array, the lasing edge mode reaches the output coupler with a fixed chirality within each ring (Fig. 3G). This shows that the topological lasing mode extends around the perimeter, and travels all the way to the output ports, whereas the lasing in the trivial case occurs in stationary localized modes. In this vein, we tested multiple samples, and found that the same features consistently emerged in a number of different designs (different resonance frequencies, couplings, etc.) in a universal manner. A video showing the behaviors of partially pumped topological and trivial arrays are provided as supplementary materials, Part 10 and more features associated with these arrays can be found in supplementary materials, Parts 3 and 5.

Introducing defects

Next, we study lasing in a topological structure and in its trivial counterpart, in the presence of defects, which are intentionally introduced into the structures. We remove specific microrings along the perimeter, where pumping is provided (i.e., we remove two gain elements). Figure 4 shows the light emission from these two types of structures. These results demonstrate that in a topological system (Fig. 4A), light is capable of bypassing the defects by penetrating into the bulk and displaying lasing in an extended edge mode of almost uniform intensity. Conversely, the intensity of the emitted light in the trivial structure is considerably suppressed (Fig. 4B), and the defects effectively subdivide the perimeter into separate regions that lase independently (both measurements are performed at identical pump power levels). Hence, the topological insulator laser is robust against defects, even when introduced into the gain regions. [Further evidence of this robustness in the presence of disorder is given in (*33*), Part 8.]

Laser based in an array of chiral S-bend elements

Having established the underlying concepts of the topological insulator laser and the promise it holds for exploring new aspects, it is interesting to discuss some of the directions these ideas can lead to. As an example, embarking on fundamental aspects such as Maxwell's reciprocity in the presence of nonlinearity, as well as on potential applications, we modify the individual resonators in the topological insulator laser,scic so as to break the symmetry between the clockwise (CW) and counter-clockwise (CCW) modes in each ring. Instead of using conventional rings we use a special S-bend design (*34*), for each primary cavity element in the topological lattice (Fig. 5, A and B). The intermediary links remain the same as in the previous designs (Fig. 1A). In this system, each laser micro-resonator selectively operates in a single spin-like manner, i.e., in either the CW or the CCW direction by exploiting gain saturation and energy recirculation among these modes. The S-chiral elements involved, in the presence of nonlinearity (gain saturation) and the spatial asymmetry of the S-bends, add unidirectionality to the topological protection of transport. In the experiments described in Fig. 5, we observe suppression of more than 12 dB between the right- and left-hand spins in each resonator [see (*33*), Part 6]. Finite difference time domain simulations also indicate that the differential photon lifetime between the right/left spins in these S-bend cavities is approximately 3ps, corresponding to an equivalent loss coefficient of 10 cm^{-1} [more details are outlined in (*33*), Part 7]. The field distribution in the prevalent spinning mode in these active S-resonators is shown in Fig. 5C, featuring a high degree of power-recirculation through the S-structure that is responsible for the spin-like

mode discrimination. The corresponding intensity profile associated with this unidirectional edge-mode energy transport is shown in Fig. 5D. In this case, energy is predominantly extracted from only one of the two out-coupling gratings (with a ~10 dB rejection ratio)—an indication of unidirectional energy flow in the rings of this topological array.

Discussion

Our all-dielectric topological insulator laser exploits the topological features to enhance the lasing performance of a 2D array of micro-resonators, making them lase in unison in an extended topologically-protected scatter-free edge mode. The observed single longitudinal mode operation leads to a considerably higher slope efficiency as compared to a corresponding topologically-trivial system. The systems described here are based on contemporary fabrication technologies of semiconductor laser, without need for magnetic units of exotic materials. Our results provide a route for developing a novel class of active topological photonic devices, especially arrays of semiconductor lasers, that can operate in a coherent fashion with high slope efficiencies.

REFERENCES AND NOTES

1. D. J. Thouless, M. Kohmoto, M. P. Nightingale, M. Den Nijs, Quantized Hall conductance in a two-dimensional periodic potential. *Phys. Rev. Lett.* **49**, 405–408 (1982). doi:10.1103/PhysRevLett.49.405
2. M. Hasan, C. Kane, Colloquium: Topological insulators. *Rev. Mod. Phys.* **82**, 3045–3067 (2010). doi:10.1103/RevModPhys.82.3045
3. X.-L. Qi, S.-C. Zhang, Topological insulators and superconductors. *Rev. Mod. Phys.* **83**, 1057–1110 (2011). doi:10.1103/RevModPhys.83.1057
4. K. V. Klitzing, G. Dorda, M. Pepper, New method for high-accuracy determination of the fine-structure constant based on quantized Hall resistance. *Phys. Rev. Lett.* **45**, 494–497 (1980). doi:10.1103/PhysRevLett.45.494
5. C. L. Kane, E. J. Mele, Quantum spin Hall effect in graphene. *Phys. Rev. Lett.* **95**, 226801 (2005). Medline
6. B. A. Bernevig, T. L. Hughes, S.-C. Zhang, Quantum spin Hall effect and topological phase transition in HgTe quantum wells. *Science* **314**, 1757–1761 (2006). doi:10.1126/science.1133734 Medline
7. M. König, S. Wiedmann, C. Brüne, A. Roth, H. Buhmann, L. W. Molenkamp, X.-L. Qi, S.-C. Zhang, Quantum spin hall insulator state in HgTe quantum wells. *Science* **318**, 766–770 (2007). doi:10.1126/science.1148047 Medline
8. F. D. Haldane, S. Raghu, Possible realization of directional optical waveguides in photonic crystals with broken time-reversal symmetry. *Phys. Rev. Lett.* **100**, 013904 (2008). doi:10.1103/PhysRevLett.100.013904 Medline
9. L. Lu, J. D. Joannopoulos, M. Soljačić, Topological photonics. *Nat. Photonics* **8**, 821–829 (2014). doi:10.1038/nphoton.2014.248
10. M. Hafezi, E. Demler, M. Lukin, J. Taylor, Robust optical delay lines via topological protection. *Nat. Phys.* **7**, 907–912 (2011). doi:10.1038/nphys2063
11. K. Fang, Z. Yu, S. Fan, Realizing effective magnetic field for photons by controlling the phase of dynamic modulation. *Nat. Photonics* **6**, 782–787 (2012). doi:10.1038/nphoton.2012.236
12. A. B. Khanikaev, S. H. Mousavi, W.-K. Tse, M. Kargarian, A. H. MacDonald, G. Shvets, Photonic topological insulators. *Nat. Mater.* **12**, 233–239 (2013). doi:10.1038/nmat3520 Medline
13. M. C. Rechtsman, J. M. Zeuner, Y. Plotnik, Y. Lumer, D. Podolsky, F. Dreisow, S. Nolte, M. Segev, A. Szameit, Photonic Floquet topological insulators. *Nature* **496**, 196–200 (2013). doi:10.1038/nature12066 Medline
14. L. Tarruell, D. Greif, T. Uehlinger, G. Jotzu, T. Esslinger, Creating, moving and merging Dirac points with a Fermi gas in a tunable honeycomb lattice. *Nature* **483**, 302–305 (2012). doi:10.1038/nature10871 Medline
15. M. Atala, M. Aidelsburger, J. T. Barreiro, D. Abanin, T. Kitagawa, E. Demler, I. Bloch, Direct measurement of the Zak phase in topological Bloch bands. *Nat. Phys.* **9**, 795–800 (2013). doi:10.1038/nphys2790
16. C. L. Kane, T. C. Lubensky, Topological boundary modes in isostatic lattices. *Nat. Phys.* **10**, 39–45 (2013). doi:10.1038/nphys2835
17. Z. Yang, F. Gao, X. Shi, X. Lin, Z. Gao, Y. Chong, B. Zhang, Topological acoustics. *Phys. Rev. Lett.* **114**, 114301 (2015). doi:10.1103/PhysRevLett.114.114301 Medline
18. R. Fleury, A. B. Khanikaev, A. Alù, Floquet topological insulators for sound. *Nat. Commun.* **7**, 11744 (2016). doi:10.1038/ncomms11744 Medline
19. Z. Yu, G. Veronis, Z. Wang, S. Fan, One-way electromagnetic waveguide formed at the interface between a plasmonic metal under a static magnetic field and a photonic crystal. *Phys. Rev. Lett.* **100**, 023902 (2008). doi:10.1103/PhysRevLett.100.023902 Medline
20. X. Cheng, C. Jouvaud, X. Ni, S. H. Mousavi, A. Z. Genack, A. B. Khanikaev, Robust reconfigurable electromagnetic pathways within a photonic topological insulator. *Nat. Mater.* **15**, 542–548 (2016). doi:10.1038/nmat4573 Medline
21. G. Jotzu, M. Messer, R. Desbuquois, M. Lebrat, T. Uehlinger, D. Greif, T. Esslinger, Experimental realization of the topological Haldane model with ultracold fermions. *Nature* **515**, 237–240 (2014). doi:10.1038/nature13915 Medline
22. M. Aidelsburger, M. Lohse, C. Schweizer, M. Atala, J. T. Barreiro, S. Nascimbène, N. R. Cooper, I. Bloch, N. Goldman, Measuring the Chern number of Hofstadter bands with ultracold bosonic atoms. *Nat. Phys.* **11**, 162–166 (2015). doi:10.1038/nphys3171
23. A. P. Slobozhanyuk, A. B. Khanikaev, D. S. Filonov, D. A. Smirnova, A. E. Miroshnichenko, Y. S. Kivshar, Experimental demonstration of topological effects in bianisotropic metamaterials. *Sci. Rep.* **6**, 22270 (2016). doi:10.1038/srep22270 Medline
24. Z. Wang, Y. Chong, J. D. Joannopoulos, M. Soljačić, Observation of unidirectional backscattering-immune topological electromagnetic states. *Nature* **461**, 772–775 (2009). doi:10.1038/nature08293 Medline
25. M. Hafezi, S. Mittal, J. Fan, A. Migdall, J. M. Taylor, Imaging topological edge states in silicon photonics. *Nat. Photonics* **7**, 1001–1005 (2013). doi:10.1038/nphoton.2013.274
26. G. Harari, M. A. Bandres, Y. Lumer, M. C. Rechtsman, Y. D. Chong, M. Khajavikhan, D. N. Christodoulides, M. Segev, Topological insulator laser: Theory. *Science* 10.1126/science.aar4003 (2018).
27. P. St-Jean, V. Goblot, E. Galopin, A. Lemaître, T. Ozawa, L. Le Gratiet, I. Sagnes, J. Bloch, A. Amo, Lasing in topological edge states of a 1D lattice. arXiv:1704.07310 [cond-mat.mes-hall] (24 April 2017).
28. M. Parto, S. Wittek, H. Hodaei, G. Harari, M. A. Bandres, J. Ren, M. C. Rechtsman, M. Segev, D. N. Christodoulides, M. Khajavikhan, Complex edge-state phase transitions in 1D topological laser arrays. arXiv:1709.00523 [physics.optics] (2 September 2017).
29. H. Zhao, P. Miao, M. H. Teimourpour, S. Malzard, R. El-Ganainy, H. Schomerus, L. Feng, Topological hybrid silicon microlasers. arXiv:1709.02747 [physics.optics] (8 September 2016).
30. G. Harari *et al*., in *Conference on Lasers and Electro-Optics* (OSA Technical Digest, Optical Society of America, paper FM3A.3, 2016).
31. S. Wittek *et al*., in *Conference on Lasers and Electro-Optics* (OSA Technical Digest, Optical Society of America, paper FTh1D.3, 2017).
32. B. Bahari, A. Ndao, F. Vallini, A. El Amili, Y. Fainman, B. Kanté, Nonreciprocal lasing in topological cavities of arbitrary geometries. *Science* **358**, 636–640 (2017). doi:10.1126/science.aao4551 Medline
33. Materials and methods are available as supplementary materials.
34. J. P. Hohimer, G. A. Vawter, D. C. Craft, Unidirectional operation in a semiconductor ring diode laser. *Appl. Phys. Lett.* **62**, 1185–1187 (1993). doi:10.1063/1.108728
35. W. D. Sacher, M. L. Davenport, M. J. R. Heck, J. C. Mikkelsen, J. K. S. Poon, J. E. Bowers, Unidirectional hybrid silicon ring laser with an intracavity S-bend. *Opt. Express* **23**, 26369–26376 (2015). doi:10.1364/OE.23.026369 Medline

ACKNOWLEDGMENTS

Funding: The authors gratefully acknowledge the financial support from Israel Science Foundation, Office of Naval Research (ONR) (N0001416-1-2640), National Science Foundation (NSF) (ECCS1454531, DMR-1420620, ECCS

1757025), U.S. Air Force Office of Scientific Research (AFOSR) (FA9550-14-1-0037), U.S.-Israel Binational Science Foundation (BSF) (2016381), the German-Israeli Deutsch-Israelische Projektkooperation (DIP) program, and Army Research Office (ARO) (W911NF-16-1-0013, W911NF-17-1-0481). **Author contributions:** All authors contributed to all aspects of this work. **Competing interests:** The authors declare no competing financial interests. **Data and materials availability:** All data needed to evaluate the conclusions in the paper are present in the paper and/or the Supplementary Materials.

SUPPLEMENTARY MATERIALS

www.sciencemag.org/cgi/content/full/science.aar4005/DC1
Materials and Methods
Figs. S1 to S11
Reference (*35*)
Movies S1 and S2

3 November 2017; accepted 17 January 2018
Published online 1 February 2018
10.1126/science.aar4005

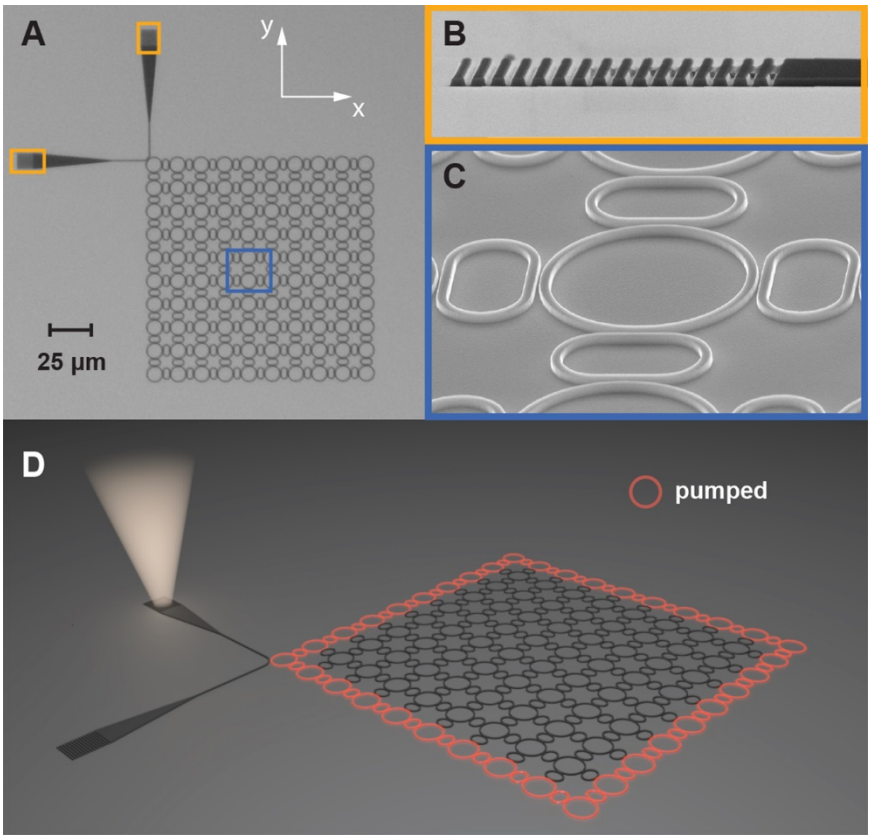

Fig. 1. Topological insulator laser: lattice geometry and associated band structure. (**A**) Microscope image of an active InGaAsP topological 10 × 10 micro-resonator array. (**B**) SEM image of the out-coupling grating structures used to probe the array at the location indicated in (A). (**C**) SEM micrograph of a unit cell comprised of a primary ring site surrounded by four identical intermediary racetrack links. (**D**) A schematic of the topological array when pumped along the perimeter so as to promote lasing of the topological edge mode.

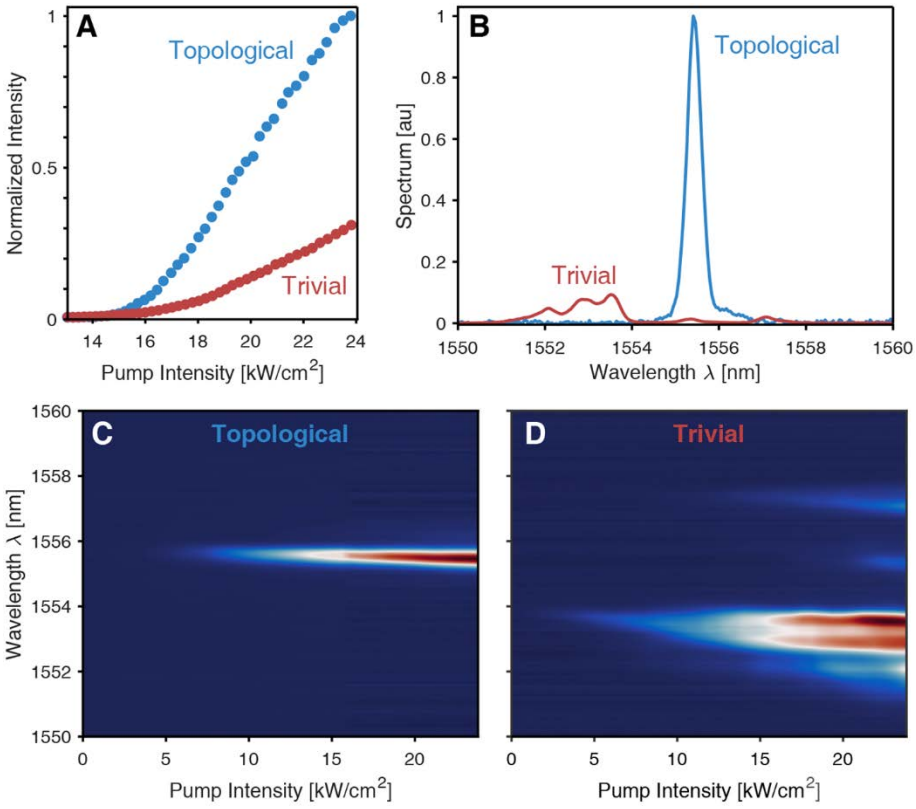

Fig. 2. Slope efficiencies and associated spectra of topological and trivial laser arrays. (**A**) Output intensity vs. pump intensity for a 10 × 10 topological array with $\alpha = 0.25$ and its corresponding trivial counterpart ($\alpha = 0$). In this experiment the enhancement of the slope efficiency is approximately 3x. (**B**) Emission spectra from a trivial and a topological array when pumped at 23.5 kW/cm^2. (**C** and **D**) Evolution of the spectrum as a function of the pumping intensity for (C) topological and (D) trivial arrays. Single-mode, narrow-linewidth lasing in (C) is clearly evident.

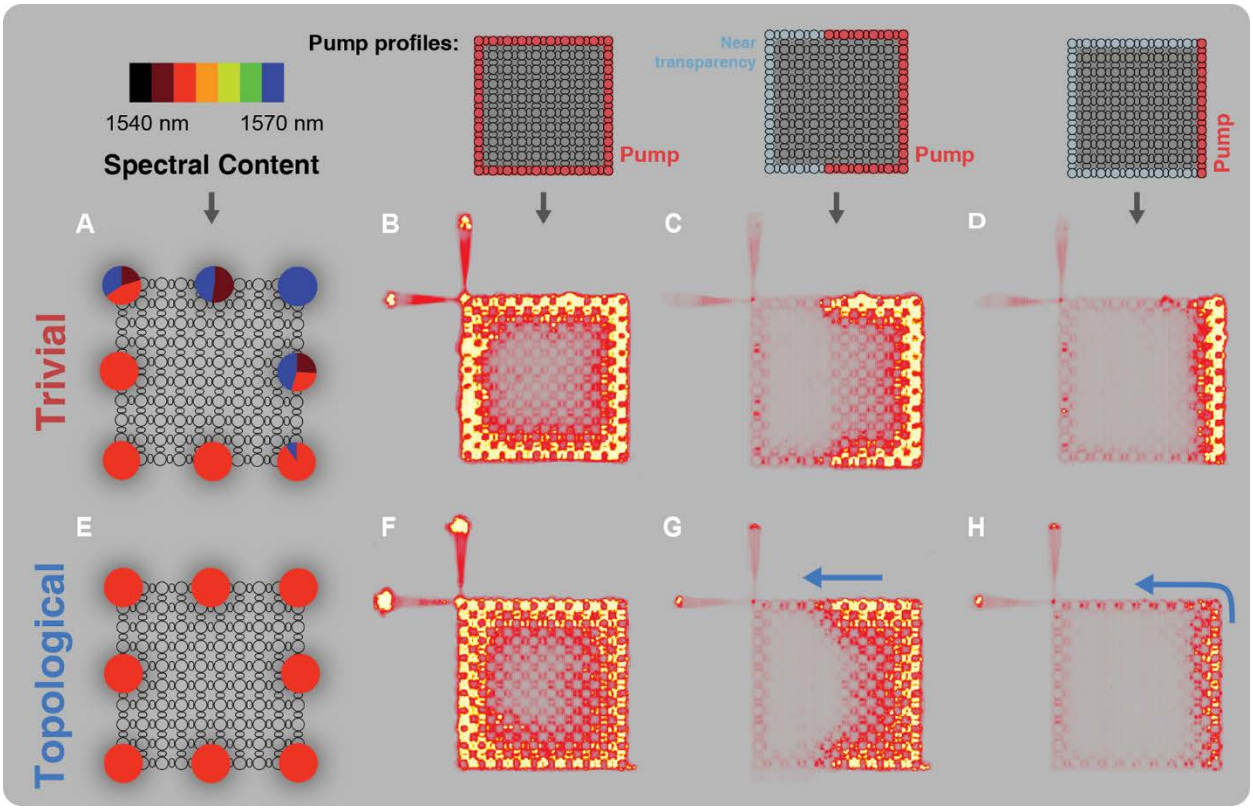

Fig. 3. Lasing characteristics of topological lattices vs. that of their corresponding trivial counterparts under several pumping conditions. Lasing in a (**B**) trivial and (**F**) topological array when their full perimeter is selectively pumped. (**A**) and (**E**) represent the spectral content as obtained from specific edge-sites of the arrays depicted in (B) and (F), correspondingly. Notice that the topological lattice remains single-moded while the trivial one emits in multiple modes. Lasing transport in a (**D**) trivial array and in a (**H**) topological lattice when the right side is pumped. The lasing edge-mode in (H) travels along the unpumped perimeter and exits mostly through the left output-grating, whereas the lasing mode in (D) never reaches the output coupler. (**C**) and (**G**) present similar results when the pumping region at the right side is further extended into the array. In (G) the lasing edge-mode again travels all the way to the output port, whereas the lasing modes of the trivial lattice never reach the extracting ports in (C). This proves that the topological mode travels around the perimeter and always reaches the output port, whereas the lasing modes of the trivial lattice are stationary. The pumping conditions are shown in the insets at the top.

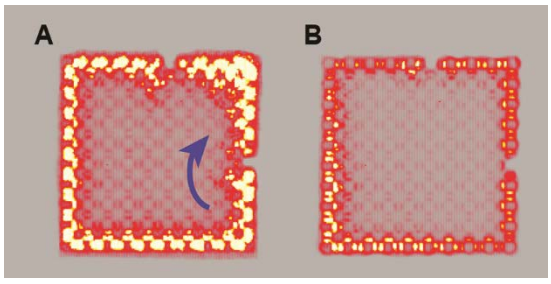

Fig. 4. Robust behavior of the lasing edge mode with respect to defects in a topological array. (**A** and **B**) Lasing response of a (A) topological and (B) trivial array in the presence of two defects intentionally inserted on the periphery, under the same pumping intensity. Note that the edge mode transport in (A) bypasses the defects, whereas in its trivial counterpart the lasing occurs from three separate sections.

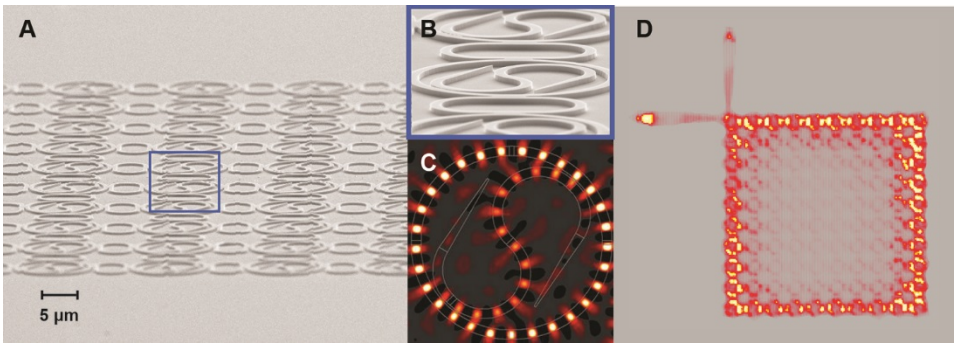

Fig. 5. Topological active array involving chiral S-micro-resonator elements. (**A**) SEM image of a 10 × 10 topological array. The primary resonators feature an internal S-bend for enforcing in this case a right-spin, while the intermediate link design is the same as in Fig. 1C. (**B**) A closeup SEM micrograph of the basic elements involved. (**C**) Field distribution in an individual S-element as obtained from FDTD-simulations. (**D**) Measured intensity profile associated with the lasing edge-mode in a topological array with $\alpha = 0.25$. In this system, the perimeter is selectively pumped, and the energy in each ring circulates in a counterclock-wise manner, as indicated by the radiation emerging from the extracting ports.

Topological insulator laser: Experiments

Miguel A. Bandres, Steffen Wittek, Gal Harari, Midya Parto, Jinhan Ren, Mordechai Segev, Demetrios N. Christodoulides and Mercedeh Khajavikhan

published online February 1, 2018